Numerical study of the influence of tungsten recrystallization on the divertor component lifetime

Alan Durif, Marianne Richou, Guillaume Kermouche, Jean-Michel Bergheau

Noname manuscript No.
(will be inserted by the editor)

Numerical study of the influence of tungsten recrystallization on the divertor component lifetime

A. DURIF · M. RICHOU · G.KERMOUCHE · J-M. BERGHEAU

Received: 15/07/2020 / Accepted: date

Abstract The thermonuclear fusion reaction between deuterium and tritium could become an alternative, sustainable and safe way to generate electricity in demand. Plasma facing components will ensure the mechanical integrity of the reactor internal walls, the heat extraction and must be compatible with the plasma operation to not compromise its exploitation. ITER and WEST (W -for tungsten- Environment in Steady-state Tokamak) components will be exposed to particles fluxes during transient loading up to 20 MW/m^2. To withstand such loading, components are actively cooled and are made with pure tungsten as material facing the plasma. Although this technology fulfills ITER's requirements, cracks appear in tungsten block under cyclic high heat flux at 20 MW/m^2. Such cracks propagate from the exposed surface to the cooling pipe. Even if the appearance of this crack does not immediately affect the component heat exhaust capability, it could limit the reactor operation. In literature, numerical models were developed and mentioned that tungsten recrystallization plays significant role on the component lifetime. To improve the numerical predictions, this paper presents an innovative tool able to take into account the progressive tungsten mechanical properties change due to recrystallization. This final model, named RXMAT, is implemented as

A. DURIF
CEA, IRFM, 13108 Saint-Paul-Lez-Durance, France
Tel.: +33442253376
E-mail: alan.durif@cea.fr

M. RICHOU
CEA, IRFM, F-13108 Saint-Paul-Lez-Durance, France

G.KERMOUCHE
Mines Saint-Etienne, CNRS, UMR 5307 LGF, Centre SMS, F – 42023 Saint-Etienne, France

J-M. BERGHEAU
University of Lyon, Ecole Nationale d'ingénieurs de Saint-Etienne, LTDS, CNRS UMR 5513, 42023 Saint-Etienne
E-mail: jean-michel.bergheau@enise.fr

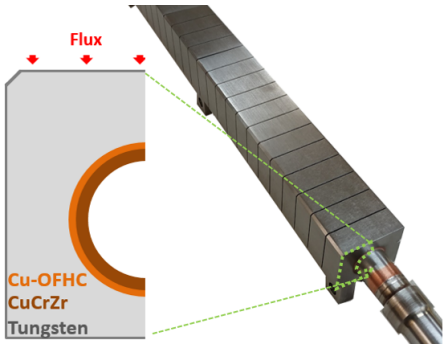

Fig. 1 Iter and WEST divertor plasma facing component technology

a user subroutine in the finite elements code ANSYS. Fueled by the tungsten recrystallization kinetics and by up to date tungsten and recrystallized tungsten elastic-viscoplastic constitutive laws, RXMAT links for the first time the tungsten recrystallized fraction evolution to a mechanical stress and strain fields.

Keywords Tungsten · Plastic strain · Recrystallization · ITER · Thermonuclear fusion · Elastic-viscoplastic

1 Introduction

To reach deuterium-tritium fusion reaction, thermonuclear reactors confine magnetically a plasma in a vacuum vessel. However, the magnetic confinement is imperfect and part of charged particles from the core plasma deviate from their trajectories, last ones following magnetic field lines. Due to the magnetic configuration, charged particles losses are directed toward the main wall, inducing thermal heat flux loading. The highest heat fluxes are located on the "Divertor" which corresponds to the lower part of the vessel. One of the Plasma Facing Components (PFCs) aim is to exhaust thermal heat flux loadings [1]. Plasma facing components (PFCs) must resist mechanically to these loadings. To exhaust the power, these components are actively cooled by water. Pure tungsten blocks are used as armor material which are bonded on a water cooling CuCrZr pipe (structural material) (figure 1) [2]. To limit the risk of tungsten delamination in case of macro-cracking, the tungsten microstructure is oriented perpendicularly to the heat loaded surface [3]. To fulfill this specification, tungsten is usually forged or rolled from sintered blocks.

ITER and WEST divertor components can be exposed to thermal heat fluxes up to 20 MW/m^2 [4] during transient which lead to the temperature increase of the tungsten loaded surface (surface exposed to particles flux) up to $2000°C$ [5–7].

Several experimental campaigns have been performed to validate such component technology, these were exposed to cyclic thermal heat flux up to 20

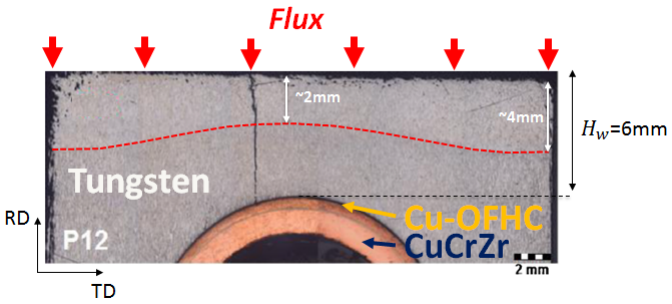

Fig. 2 Macro-crack of tungsten block observed after 1000 cycles thermal cycles at 10 MW/m^2 + 1000 thermal cycles at 15 MW/m^2 + 500 thermal cycles at 20 MW/m^2) [12]

MW/m^2 [8–11]. Here, a thermal cycle is defined as 10s of charge (exposure to heat flux) and 10 s of cooling (10 s ON / 10 s OFF). Although this component technology fulfills the ITER's requirements (5000 thermal cycles at 10 MW/m^2 + 300 thermal cycles at 20 MW/m^2), damages have been highlighted over thermal cycles. Cracks appear in tungsten blocks after few tens (up to few hundreds) of thermal cycles at 20 MW/m^2 and propagate from the exposed loaded surface to the cooling pipe [12].

In order to identify the damage process of such components, post-mortem analyzes were carried out [7,12]. These experiments revealed a change of the tungsten microstructure (drop of hardness) near the loaded surface. It was shown that tungsten recrystallized up to 2 mm in the block center and up to 4 mm on the block external borders (figure 2 [12]). The fracture surfaces presented in [12] and [13] also demonstrate a ductile failure in the near loaded surface which reveals that the related damage process is governed by plasticity. The appearance of this crack, does not immediately affect the component heat exhaust capability. Nevertheless, this leads to mechanical integrity issues induces by tungsten block delamination and/or misalignment and could limit the plasma operation.

To optimize the components use, this paper aims at presenting a numerical tool which leads to predict numerically PFCs lifetime. In this study, the component lifetime is estimated as the time required to nucleate a crack in the tungsten block.

The lifetime is estimated by the Manson-Coffin (MC) laws which link the equivalent plastic stain increment to the number of cycle to failure (Nf) [14]. MC relationships are known for tungsten (W) at 20°C and 815°C and for recrystallized tungsten (RxW) at 815°C. To estimate the fatigue lifetime a common way in literature leads to use half of the equivalent plastic strain increment (named $\Delta p'$ in the following presented numerical results) into the MC relationships [14,21].

Several numerical models were developed to assess lifetime [6,14,15]. These aim at estimating the equivalent plastic strain increment within the tungsten block obtained after each thermal cycle in order to estimate the component

lifetime from the use of these MC relationships by taking into account the impact of the Ductile to Brittle Transition Temperature (DBTT). Throughout these studies it was showed that a decoupled approach (thermomechanics and metallurgy) on a stationary cycle make it possible to better understand the component damage process and give preliminary lifetime predictions [14,15]. These results forge a path toward the development of a coupled approach to improve the prediction aspect.

Existing models do not take into account the progressive change of tungsten mechanical properties due to recrystallization over thermal cycles. To integrate recrystallization effect on loss of mechanical properties during heat loading, this paper presents an innovative developed numerical model. This model is implemented in the finite element code ANSYS thanks to a user subroutine named RXMAT in the sequel.

In the first part of this paper, the overall operation, the assumptions and the constitutive equations related to the RXMAT model are presented. In the the second part, RXMAT parameters are identified. As the last part of this paper, an application is presented and highlights the added values of this new numerical tool.

2 RXMAT constitutive equations

2.1 General overview of the model

As highlighted in the previous part, tungsten recrystallizes under thermal cycles. Here, an index notation is used to separate the state variables as well as the parameters related from each material: W, for the as-received material and Wrx, for the recrystallized one. Infinitesimal transformations are assumed in this study.

It is important to note that once recrystallized, the tungsten microstructure cannot evolve anymore. More clearly, only one microstructural transformation is considered: from as-received tungsten to recrystallized tungsten. The tungsten recrystallization is a temperature dependent phenomenon which occurs with a certain kinetics.

In this paper, the material behavior is represented by a two parallel branches model (figure 3). Each branch representes the behavior of one of the tungsten states. The total strains (ε) are assumed equal in the two branches:

$$\varepsilon_{\mathbf{w}} = \varepsilon_{\mathbf{wrx}} = \varepsilon \tag{1}$$

and the stress (σ) is given by the following rule of mixture:

$$\sigma = X\sigma_{wrx} + (1 - X)\sigma_w \tag{2}$$

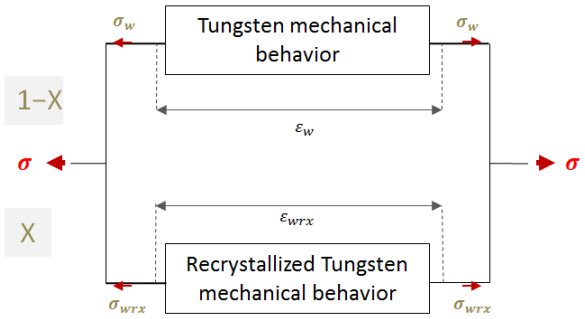

Fig. 3 Overall operation of RXMAT

Where:
-σ_w and σ_{wrx} correspond to the stress obtained from the branch W and from branch Wrx, respectively (figure 3)
- X, input of the model corresponds to the recrystallized fraction of the material which can evolve from 0 to 1.

This rule of mixture allows the progressive change of the material properties (from the as-received material to the recrystallized material).

Recent studies revealed that tungsten presents an elastic-viscoplastic behavior and presents an elastic-viscoplastic behavior with strong hardening once recrystallized from $500°C$ to $1150°C$ [18]. Based on these experimental observations, **an elastic-viscoplastic model is considered for tungsten and recrystallized tungsten**.

2.2 Elastic-viscoplastic constitutive equations

Constitutive equations are chosen according to the stress-strain $(\sigma - \varepsilon)$ curves presented in [15].

In the small transformation assumption, the total strain tensor (ε) is decomposed as follow:

$$\varepsilon = \varepsilon^e + \varepsilon^p + \varepsilon^{th} \tag{3}$$

Where:
- ε^e defines the elastic strains tensor
- ε^p defines the plastic strains tensor
- ε^{th} defines the thermal strains tensor as:

$$\varepsilon^{th} = (T_s - T_0) \times \beta(T_s) \tag{4}$$

-T_0 corresponds to the initial material temperature prior to plasma choc ($T_0 = 120°C$)
-T_s defines the tungsten surface block temperature
- β defines the tungsten thermal expansion coefficient [19] which may depend on Ts.

The Hooke's law parameters (equation 5) conventionally used in the literature to describe the elastic behavior of a material are identified from the data available in [19]:

$$\sigma = C : \varepsilon^e = \lambda tr(\varepsilon^e).I + 2\mu\varepsilon^e \tag{5}$$

Where:
-C defines the material elasticity (4th order tensor)
- λ and μ correspond to the Lamé coefficients
- I defines the identity matrix

A unified elastic-viscoplastic model is considered. The time dependent plastic strain will be noted (ε^p).

To introduce the viscoplasticity within the mechanical behavior model, a Norton-Hoff type law is used:

$$\dot{p} = |\dot{\varepsilon}^p| = < \frac{f(\sigma, \chi)}{K} >^n \tag{6}$$

Where:
- K and n define two parameters
- $f(.)$ defines the plastic criterion
- χ defines the kinematic hardening variable
- the symbol $\langle\rangle$ defines the Macauley bracket meaning that:
$\langle x \rangle = \left\{ \begin{array}{ccc} x & if & x > 0 \\ 0 & else & \end{array} \right\}$
- σ defines the material stress tensor
-$\dot{p}$ corresponds to the accumulated equivalent plastic strain rate as:

$$\dot{p} = \sqrt{\frac{2}{3}\dot{\varepsilon}^p : \dot{\varepsilon}^p} \tag{7}$$

The von Mises criterion is commonly used in the literature for metallic soft materials [22]. Its expression is a function of the equivalent von Mises stress defined as follow:

$$J(\sigma) = \sqrt{\frac{3}{2}\mathbf{S} : \mathbf{S}} \tag{8}$$

Where:
-$J(.)$ defines the von Mises invariant
-S corresponds to the deviatoric stress tensor defined here below:

$$S = \sigma - \frac{1}{3}tr(\sigma) \tag{9}$$

In this study, purely kinematic hardening is assumed. This hypothesis is made based on the cyclic tensile curve obtained for recrystallized tungsten at $800°C$ [25]. Therefore, the plasticity criterion takes the form:

$$f(\sigma, \chi) = J(\sigma - \chi) - \sigma^y \tag{10}$$

Where:
- σ^y defines the yield stress of the material

Following the normality rule, $\dot{\varepsilon}^p$ is defined as [22]:

$$\dot{\varepsilon}^p = \frac{3}{2}\dot{p}\frac{S - \chi}{J(S - \chi)} \tag{11}$$

The $\sigma - \varepsilon$ curves displayed in [15] reveal nonlinear hardening for recrystallized tungsten. The introduction of an Armstrong-Frederick kinematic hardening variable could be considered [22]. However, regarding the expected plastic strain range (0.325% per thermal cycle [14]), linear kinematic hardening is assumed for recrystallized tungsten:

$$\chi = \frac{2}{3}H\alpha \tag{12}$$

Where:
- H is defined based on the material Young modulus (E) and the tangent modulus (E_T):

$$H = \frac{EE_T}{E - E_T} \tag{13}$$

- α is the internal variable associated with kinematic hardening [22]. When no recrystallization occurs, we have for a linear kinematic hardening:

$$\alpha = \varepsilon^p \tag{14}$$

Equation 12 assumes that χ depends only on the plastic strains tensor. However, during the recrystallization process, the evolution of α between time t and $t + dt$ must take account of [24]:

- The hardening of the recrystallized fraction preexisting at time t
- The non recrystallized fraction that becomes recrystallized between t and $t + dt$ and that is supposed to be virgin of any hardening. Equation (14) is therefore modified in the following way:

$$\dot{\alpha} = \dot{\varepsilon^p} - \frac{\dot{\chi}}{\chi}\alpha \tag{15}$$

The constitutive equations are integrated step by step using a fully implicit algorithm. The principle of the method is to reduce as much as possible the set of equations to be solved [23]. In the present case, at each time step, the set of equations is reduced to a single scalar equation of a scalar unknown namely the accumulated equivalent plastic strain increment, Δp. The resolution method is detailed in appendix A.

The parameters E, ν and α are assumed identical for tungsten and recrystallized tungsten. This assumption is consolidated as no metallurgical phase change over the recrystallization process is noticed. Besides, experiments performed by D.Serret et al highlighted that the tungsten thermal properties remain stable prior to and after recrystallization [29]. Their related values are given in [19]. In this manner, considering the following Hooke's laws:

$$\sigma_w = C : (\varepsilon - \varepsilon^{th} - \varepsilon^p_w) \tag{16}$$

$$\sigma_{wrx} = C : (\varepsilon - \varepsilon^{th} - \varepsilon^p_{wrx}) \tag{17}$$

and equations 1 and 2, it is assumed that p (equation 7) can be estimated from a rule of mixture:

$$\sigma = C : \left[\varepsilon - \varepsilon^{th} - \underbrace{(X\varepsilon^p_{wrx} + (1-X)\varepsilon^p_w)}\right] \tag{18}$$

2.3 Anisothermal recrystallization modeling

Let X be the tungsten recrystallized fraction, the recrystallization kinetics can be described using the phenomenological Johnson-Mehl-Avrami-Kolmogorov (JMAK) model which gives X evolution at a constant temperature [26–28]:

$$X(t) = 1 - \exp(-b^{n_{JMAK}}(t - t_{inc})^{n_{JMAK}}) \tag{19}$$

Where:
-b et n_{JMAK} define two temperature dependent parameters. n_{JMAK} is considered as constant and is set to 1.098 [30].
-t_{inc} defines the material incubation time. This temperature dependent parameter corresponds to the necessary time required for the nucleation of the first nucleus (recrystallized grains):

$$t < t_{inc} \Longrightarrow X = 0$$

$$t > t_{inc} \Longrightarrow 0 < X \leq 1$$

Under plasma operation, PFCs temperature change from $20°C$ to $2000°C$ cyclically maintained for several seconds [5]. A different models of metallurgical transformations under anisothermal conditions have been proposed [20,31–33]. In the present case, we use the formulation of Pumphey et al [32] which is named Anisothermal JMAK Model (AJM) in the sequel.

AJM introduce a threshold (Δinc) which assesses whether the material is in its incubation or recrystallization phase. It is based on an expression using the incubation time ($tinc$). From a numerical modeling point of view, the AJM considers an isothermal "plateau" between two time steps (t_i and t_{i+1}) for which temperatures are different. $Tp(t = ti)$ is defined as the temperature during this "plateau", which is an average of the temperatures preceding and following this plateau:

$$Tp(t_i) = \frac{Tp(t_i) + Tp(t_{i+1})}{2} \tag{20}$$

This temperature is applied during Δt ($t_{i+1} = t_i + \Delta t$). In the case of anisothermal loading, $tinc$ and b from the JMAK model are assumed to be temperature dependent [20]. Here, Δinc is defined as the material incubation fraction:

$$\Delta inc = \sum \frac{\Delta t}{t_{inc_{Tp(t)}}} \tag{21}$$

Where:
$tinc_{Tp(t)}$ defines the incubation time estimated at the average temperature $Tp(t)$.

Once $\Delta inc = 1$, the incubation time is reached and the recrystallization process starts. X is provided according to the equation 22:

$$\Delta inc \Longrightarrow X(t) = 1 - exp(-(b_{T_p(t)} \times t)^{n_{JMAK}}) \tag{22}$$

In order to describe the evolution of X occurring at $t + \Delta t$, over an anisothermal path, it is necessary to introduce the notion of fictive time (t^*) which corresponds to the time needed at $Tp(t + \Delta t)$ to obtain $X(t)$. From equation 22, t^* is defined as:

$$t^* = [ln(\frac{1}{(1-X(t))})]^{\frac{1}{n_{JMAK}}} \times * \frac{1}{b_{T_p(t+\Delta t)}} \quad (23)$$

Finally, the anisothermal JMAK equation is given [20,31,32]:

$$X(t+\Delta t) = 1 - exp(-(b_{T_p(t+\Delta t)} \times (t^* + \Delta t))^n) \quad (24)$$

With t*=t for isothermal paths.

3 Determination of model parameters

3.1 Anisothermal JMAK parameters

Up to now, recrystallization kinetics of relevant tungsten are known on restricted temperature range from $1150°C$ to $1350°C$ [30]. Aware about the fact that tungsten recrystallization became a key parameter to develop and optimize the use of PFCs, several experimental campaigns were launched recently [18,34].

Here, Arrhenius laws given in [18] to describe the evolution of b and $tinc$ parameters are considered:

$$ln(\frac{1}{b}) = 2.41 \times \frac{10000}{T} - 9.62 \quad (25)$$

$$ln(tinc) = 3.28 \times \frac{10000}{T} - 16.79 \quad (26)$$

These Arrhenius laws allow the estimation of b and $tinc$ parameters between $1350°C$ and $1800°C$. No extrapolation is allowed using these laws [18].

3.2 Elastic-viscoplastic parameters

3.2.1 Identification method and results

In this section, the parameters related to the elastic-viscoplastic model are determined (K, n, σ^y and E_T).

The parameter E_T (tangent modulus) represents the slope of the $\sigma - \varepsilon$ curve plastic part. Usually, E_T is determined between the material yield strength at 0.2% offset (Y_s) and a stress value chosen at a certain level of strain. It is proposed here to estimate E_T as the average slope between Ys and $\sigma_{\varepsilon^p=2\%}$, which corresponds to the stress value measured at 2% plastic strain (figure 4). 2% is relevant regarding the thermal strain increment expected during a representative thermal cycle at 20 MW / m^2 (taking $\Delta T = 4000°C$ corresponding to the expected temperature variation over the thermal cycle at 20 MW / m^2 and β equal to $5{,}08.10^{-6}K^{-1}$ [19].

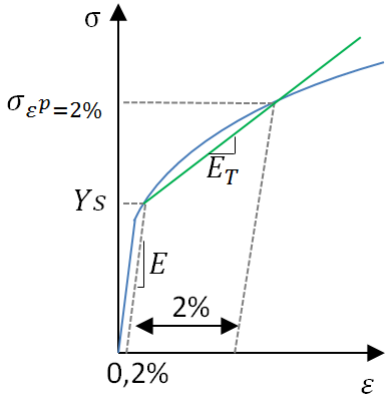

Fig. 4 Identification of Y_s and E_T parameters based on $\sigma - \varepsilon$ curves

$E_{T(2\%)}$ (GPa)	Tungsten			
Temperature	$500°C$	$750°C$	$950°C$	$1150°C$
6.10^{-1} s^{-1}	0.77	0.75	-	-
6.10^{-2} s^{-1}	1.52	0.55	-	-
6.10^{-3} s^{-1}	0.94	-	-	-
Average	0.85		-	-

$Y_{s(0.2\%)}$ (MPa)	Tungsten			
Temperature	$500°C$	$750°C$	$950°C$	$1150°C$
6.10^{-1} s^{-1}	678	555	501	459
6.10^{-2} s^{-1}	570	544	506	443
6.10^{-3} s^{-1}	559	529	498	426

$E_{T(2\%)}$ (GPa)	Recrystallized tungsten			
Temperature	$500°C$	$750°C$	$950°C$	$1150°C$
6.10^{-1} s^{-1}	9.12	5.28	5.18	4.59
6.10^{-2} s^{-1}	8.44	5.20	4.66	4.12
6.10^{-3} s^{-1}	5.35	5.23	4.12	3.55
Moyenne	7.64	5.24	4.65	4.09

$Y_{s(0.2\%)}$ (MPa)	Recrystallized tungsten			
Temperature	$500°C$	$750°C$	$950°C$	$1150°C$
6.10^{-1} s^{-1}	46	59	50	58
6.10^{-2} s^{-1}	37	48	35	43
6.10^{-3} s^{-1}	61	39	41	49

Table 1 E_T and Y_s paramters obtained for tungsten and recrystallized tugsten from $500°C$ to $1150°C$

E_T are presented in the table 1. Because of the softening phenomena observed for tungsten at $900°C$ and $1150°C$ [15], E_T is only estimated at $500°C$ and $750°C$. For tungsten, it is assumed that E_T is constant and equal to the average of E_T obtained at $500°C$ and $750°C$ ($E_T = 0.85GPa$). For the re-

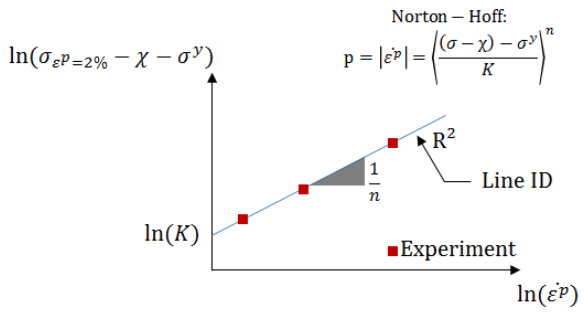

Fig. 5 Identification method

crystallized tungsten, the evolution of E_T as a function of the temperature is given here below:

$$E_T(Pa) = -2947462,7 \times T + 74,63.10^8 \tag{27}$$

To identify the parameters K and n, the Norton-Hoff law (equation 6) is written as follow:

$$ln(\sigma - \chi - \sigma^y) = \frac{1}{n} ln(\dot{\varepsilon}^p) + ln(K) \tag{28}$$

In a uniaxial case, equation 28 allows the estimation of the parameters $\frac{1}{n}$ and $ln(K)$ (figure 5). From the $\sigma - \varepsilon$ curves obtained, this identification method allows the estimation of the viscoplastic parameters related to tungsten and recrystallized tungsten per studied temperature and per strain rate ($\dot{\varepsilon}^p$). Usually, the parameter σ^y which is temperature dependent is identified from relaxation tests [35]. Due to the lack of data, σ^y is determined by maximizing the correlation coefficient, R^2, estimated for each line (line ID, figure 5) for each temperature.

To apply this identification method, several assumptions have to be made. Taking into account a weak E_T evolution over the strain rate range, it assumed that E_T is only temperature dependent.

Table 2 presents the values obtained for each parameters (σ^y, K, and n) and give their linear approximation over the studied temperature range.

The evolution of the parameters (σ^y, K, and n) have to be monotonous with the increase of the temperature [22]. However, K and n evolution are not monotonous for the recrystallized tungsten. In the future, further tests could be performed to obtain more relevant estimation. In a perspective of a numerical use, these parameters are considered strictly positive and are consequently not extrapolated for both tungsten and recrystallized tungsten.

Tungsten				
Temperature	$500°C$	$750°C$	$950°C$	$1150°C$
σ^y, (Pa)	552.10^6	524.10^6	-	-
K	$166{,}91.10^6$	$352{,}87.10^5$	-	-
n	1.75	2.63	-	-
$\sigma^y = -112000 \times T + 608.10^6$ $K = -526518,72 \times T + 430.10^6$ $n = 0.0035 \times T - 0.027$				

Recrystallized Tungsten				
Temperature	$500°C$	$750°C$	$950°C$	$1150°C$
σ^y, (Pa)	60.10^6	40.10^6	30.10^6	30.10^6
K	$130{,}52.10^6$	$79{,}72.10^6$	$71{,}12.10^6$	$84{,}99.10^6$
n	3,83	10,78	9,50	8,72
$\sigma^y = -4743,94 \times T + 7,97.10^6$, $R^2 = 0.87$ $K = -71003,7 \times T + 151052482,8$, $R^2 = 0.55$ $n = 0.0067 \times T + 2.58$, $R^2 = 0.38$				

Table 2 K, n and σ^y obtained for tungsten and recrystallized based on $\sigma-\varepsilon$ curves presented in appendix [15,18]

4 Application: Finite element analysis

4.1 Geometry, meshing material properties

A first use of RXMAT is proposed in order to evaluate the added value of this new tool comparing to published data ([15]).

For this, it is proposed to use the finite element model initially developed by M.Li et al (presented in [14] and [15]). Dimensions are reminded in figure 6.

The mechanical properties taken into account are presented in previous sections. Concerning Cu-OFHC and CuCrZr, their mechanical properties are extracted from [19]. Here, the stresses as well as the strains generated within these two materials are not studied.

For each simulation, on the upper surface of the tungsten block a uniform thermal heat flux (20 MW/m^2) is cyclically (10 s ON / 10 s OFF) applied (figure 6). The boundary conditions applied in [15] are preserved. Free nodes displacements are allowed only in the z direction for surface with chequered pattern (figure 6). Two symmetry plans are also used (YZ and XY) and allow the modeling of a quarter part of the tungsten block. To obtain consistent results, it was necessary to constrain the tungsten by fixing a point at the bloc bottom. Reference temperature of zero thermal strain is set equal to $450°C$. Mesh sensitivity study is presented in appendix B and shows that upcoming results are robust and mesh independent.

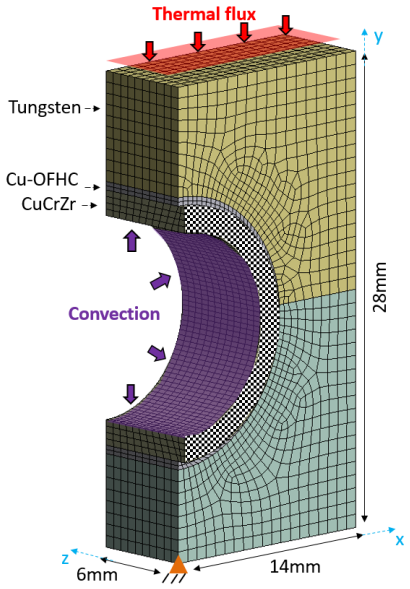

Fig. 6 Finite element model

4.2 Studied cases

The table 3 provides a summary of the simulations performed in this chapter. These are more widely described here below:

1. The **EVP-REF** simulation assumes an as-received tungsten block. This numerical simulation aims at estimating Δp based on the use of an elastic-viscoplastic (EVP) model behavior for tungsten. To neglect the recrystallization phenomenon and estimate Δp for as-received material, t_{inc} parameter is set equal to infinity in the RXMAT tool.
2. The **EVP-REFx** simulation assumes a fully recrystallized tungsten block. This numerical simulation aims at showing the influence of the use of an EVP model behavior for recrystallized tungsten on Δp estimation. For that, comparison is made between Δp obtained from **EVP-REF** simulation. To estimate Δp for a fully recrystallized tungsten, the state variables, X and Δinc, are set equal to 1.
3. The **EVP-FULL** simulation aims at demonstrating the impact of the X progressive change on Δp estimation over thermal cycles. For this, the Δp evolution is studied as a function of X. 40 thermal cycles are simulated.

4.3 Numerical results

The thermal responses of the numerical simulations are displayed in [15].

The figure 7 shows that the maximum plastic strain is estimated at the upper part of the tungsten block center. This observation is consistent with the

	Microstructural state of the tungsten	Number of thermal cycles at 20 MW/m^2
EVP-REF	Tungsten	5
EVP-REFx	Recrystallized tungsten	5
EVP-FULL	Progressive recrystallization of the tungsten block	40

Table 3 Overview of the performed simulations

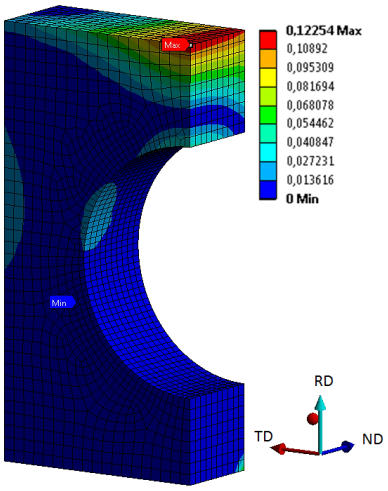

Fig. 7 p estimated from **EVP-REFx** simulation after 5 thermal cycles at 20 MW/m^2

location of macro-cracks observed experimentally (figure 2). In the upcoming sections, X, p and $\Delta p'$ are given at this position. Note that the maximum temperature reached at this position is around 1800°C.

The figure 8 shows that $\Delta p'$ stabilizes after 4 thermal cycles for the **EVP-REFx** simulation. This observation is also valid for the **EVP-REF** simulation. Consequently, for these two simulations, the $\Delta p'$ presented are those obtained at the 5th thermal cycle.

4.3.1 Influence of elastic-viscoplastic behavior on equivalent plastic strain increment

$\Delta p'$ obtained for the numerical simulations **EVP-REF** and **EVP-REFx** are presented in table 4. This table also indicates that between 10.5% and 12% $\Delta p'$ fraction (depending on the microstructural state of the material) is generated while the material temperature is lower than the DBTT (350°C).

The figures 9 and 10 show Δp evolution during the 5th thermal cycle for the **EVP-REF** and **EVP-REFx** simulations, respectively. These curves are expressed as function of the fraction of thermal cycle.

As shown in figure 9, during the transient phase, Δp is equal to 0 until the temperature reach 800°C (point A figure 9). Then, Δp increases until it becomes constant as soon as the temperature variation becomes small from

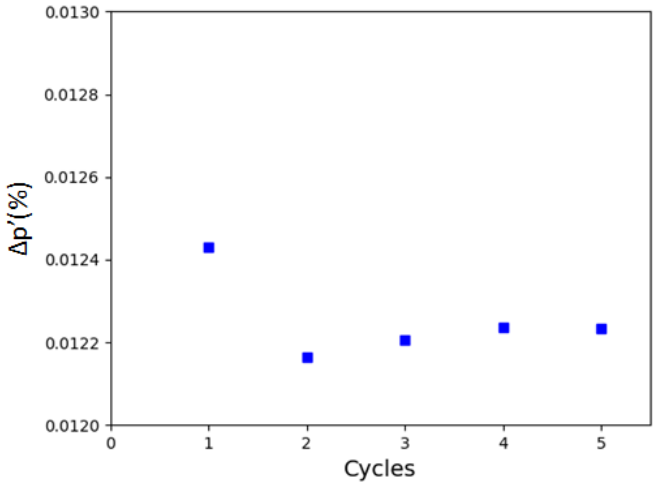

Fig. 8 $\Delta p'$ obtained over the 5 thermal cycles at 20MW/m^2 for the simulation **EVP-REFx**

	EVP-REF	**EVP-REFx**
$\Delta p'(\%)$	0.85	1.13
$\Delta p'_{<350°C}\%$	10.5	12
$N_{1<350°C}$	31	7
$N_{2>350°C}$	3867	176
$N_{F350°C}$	**30**	**6**

As reminder: $\frac{1}{Nf} = \frac{1}{N1} + \frac{1}{N2}$ [14]

Table 4 Summary of $\Delta p'$ obtained and the related lifetime assuming tungsten DBTT equal to 350°C for the simulations **EVP-REF** et **EVP-REFx** after 5 thermal cycles at 20 MW/m^2 .

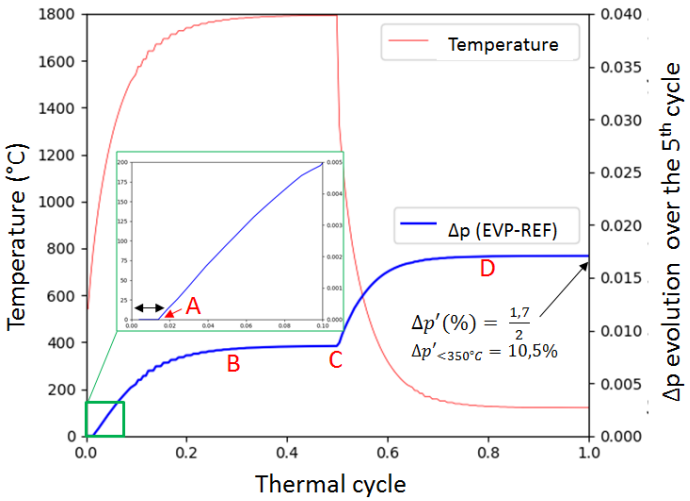

Fig. 9 p evolution during the 5th thermal cycles for the simulation **EVP-REF**

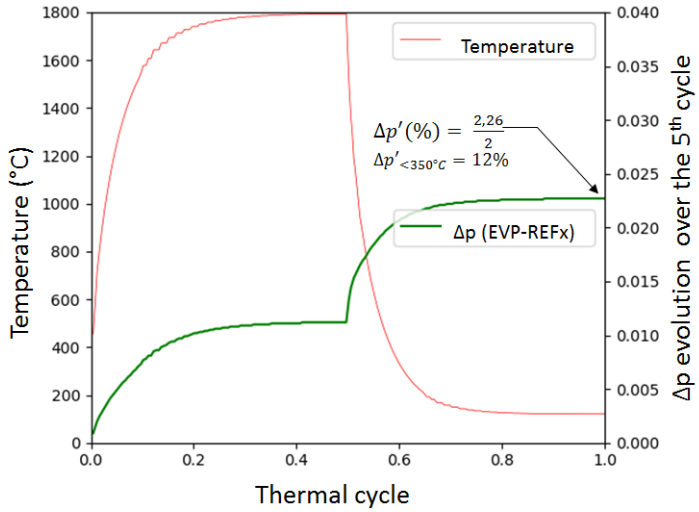

Fig. 10 p evolution during the 5th thermal cycles for the simulation **EVP-REFx**

0.3 (point B) to 0.5 cycle (point C). During the cooling phase, *Deltap* starts to increase once the temperature reaches $1400°C$ and become stable under the DBTT at 0.8 cycle (point D). Contrary to the cooling phase, no plastic strain occurs below the tungsten DBTT during the heating phase. This observation highlights that the cooling phase plays a major role in the tungsten damage process.

Concerning the **EVP-REFx** simulation, the figure 10 reveals that plastic flow occur below the DBTT upon loading. The transient heating and cooling phases have the same impact on Δp evolution.

The table 4 reveals that Δp is approximately 25% more important when taking into account elactic-viscoplastic behavior rather than only elastic behavior.

4.3.2 X evolution influence on $\Delta p'$ (EVP-FULL simulation)

The figure 11 (a) presents the X evolution for the simulation **EVP-FULL**. It can be observed that the tungsten block start to recrystallize from the first thermal cycle and is fully recrystallized during the 29th thermal cycle.

The figure 11 (b) reveals that $\Delta p'$ depends on X. Indeed, we notice that $\Delta p'$ increases between the 2nd (0.71%) and the 24th thermal cycle (0.97%) while X (note Xm which defines the average of X on a thermal cycle.) increases from 0.08 to 0.95. A very slight decrease of the plastic strain increment per cycle is observed after the 24th cycle (X=0.95). It can be assumed that the tungsten is fully recrystallized at this stage. $\Delta p'$ tends to stabilize from the 38th cycle at 0.945%.

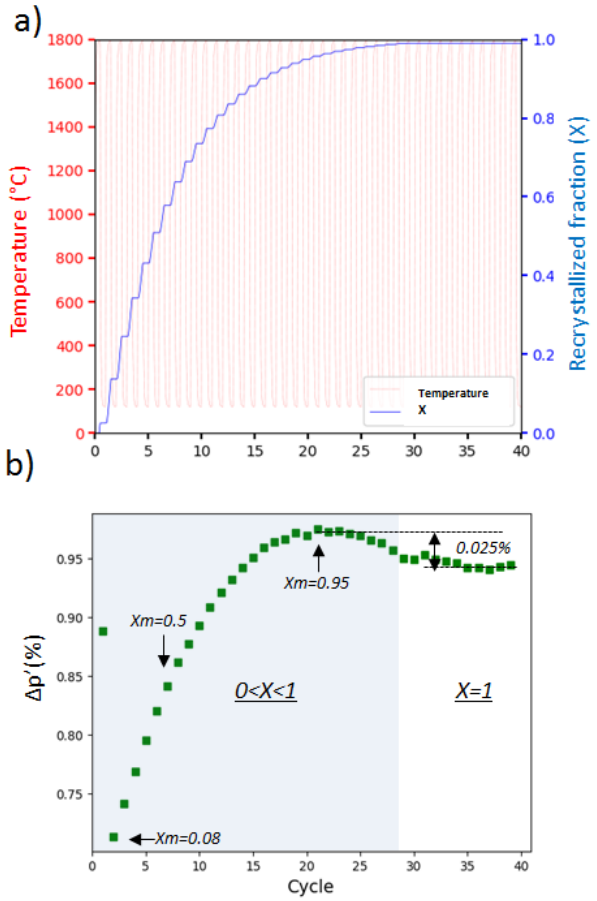

Fig. 11 X evolution over 40 thermal cycle (a) / Δp evolution over 40 thermal cycles at 20MW/m^2 (b). Xm defines the average of X on a thermal cycle.

The fraction of $\Delta p'$ generated at $T < 350°C$ is studied and shows that 11 % of $\Delta p'$ is generated at $T < 350°C$. This result is estimated on the 6th thermal cycle and is representative for the other cycles at +/- 1 %.

4.4 Component lifetime estimations

As a reminder, the tungsten DBTT is assumed equal to $350°C$.

Obtained results reveal that $\Delta p'$ is not constant during the recrystallization process thereby D is introduced and defines the fatigue damage accumulation $(0 < D < 1)$ as:

$$D_i = \frac{Ni}{N_{f_i}} \Longrightarrow \sum_i D_i = 1 \tag{29}$$

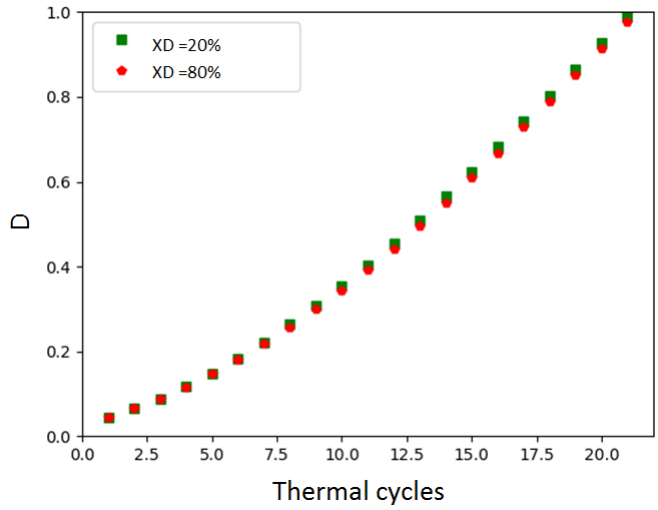

Fig. 12 D estimated over the 40 thermal cycles for the simulation **EVP-FULL**

Where:
-D_i defines the fatigue damage accumulation estimated during the ith thermal cycle
- N_i correspond to the number of cycle achieved with N_{f_i} defined from the laws of Manson Coffin

D is based on the assumption of linear cumulative damage (Palmgren-Miner's linear cumulative rule)[22]. Once $D = 1$, the appearance of the crack within the tungsten block is assumed. In the **EVP-FULL** simulation, the tungsten block is partially recrystallized up to the 28th cycle. We introduce a threshold (XD) beyond which N_f is estimated from the use of the Manson-Coffin data known for recrystallized tungsten. When X become greater than XD, then the material is assumed recrystallized in the calculation of N_f.

D evolution is presented in figure 12 assuming several thresholds (20% and 80%). This figure shows that D reaches 1 in the 21st cycle. 21 cycles corresponds to the estimated component lifetime whatever XD chosen. This reveals that XD has a negligible impact on the D evolution. Because of the large fraction (11%) of $\Delta p'$ generated for a temperature lower than the DBTT, the block damage process is governed by the plastic strain generated at low temperature. Due to the fact that the Manson-Coffin law is missing at $20°C$ for recrystallized tungsten, XD defined does not play a major role. Nevertheless, this observation give the opportunity to emphasize the lack of tungsten fatigue data. Comparing lifetime obtained for **EVP-REF** (30 cycles), **EVP-REFx** (6 cycles) and **EVP-FULL** (21 cycles) simulations, it can be notice that the material microstructural state plays a major role on the final result. It was shown that $\Delta p'$ depend on X and on the X gradient generated within the tungsten block. The time require to recrystallize the tungsten block has conse-

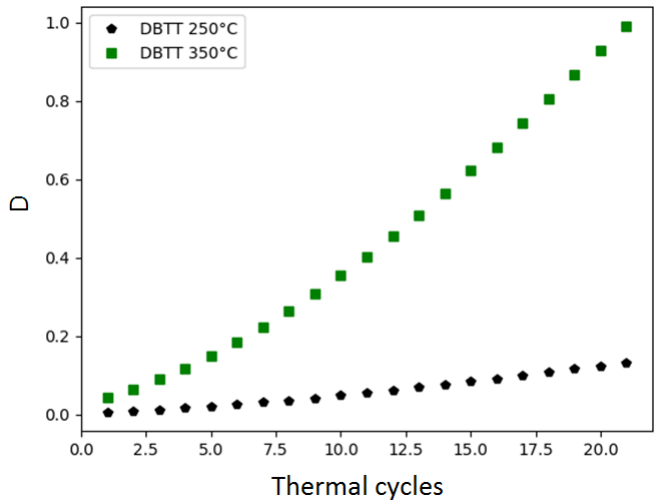

Fig. 13 Evolution of D for the simulation **EVP-FULL** assuming two tungsten DBTT ($350°C$ and $250°C$) and $XD = 20\%$.

quently a direct impact on the component lifetime. In the near future, several numerical simulations could be achieved. These simulations could reveal the impact of the recrystallization kinetics on the component lifetime. Finally, if the tungsten DBTT is assumed equal to $250°C$, the fraction of $\Delta p'$ generated below this temperature decreases from 11% to 6%. The figure 13 highlights the impact of such assumption on the evolution of D over the thermal cycles. This last result, shows once again, that the tungsten DBTT has to be more precisely identified to provide relevant component lifetime estimation. Assuming the tungsten DBTT equal to $250°C$, $D = 0.12$ after 21 thermal cycles.

4.5 Discussions

This first RXMAT application demonstrates that taking into account the progressive change of the elastic-viscoplastic tungsten properties represents significant added value in the $\Delta p'$ and N_f estimations over the thermal cycles. It can be noticed that EVP_REFx overestimates $\Delta p'$. This means that the thermomechanical history influences $\Delta p'$. In a dimensional approach, conservative study can help to discriminate between several concepts. In that case, this overestimation is too important to predict consistently the evolution of plastic strains and estimate the relevant component lifetime. As a final opening, it can be noticed that strong hypothesis are made in this paper. It is assumed that only the heat flux has a direct consequences the component lifetime. This hypothesis is true in the context of high heat flux test campaigns carried out to experimentally qualify these components under representative thermal loads. However, in reactor environment, such components are also exposed to chemi-

cal (diffusion of chemical species: D, T and He) and neutron stress [37]. Recent developments for the ITER application make it possible to numerically model the phenomenon of diffusion and trapping of hydrogen isotopes within the tungsten [38]. However, these recent works do not allow a coupling with the stress and strain mechanical fields to assess their impact on the component lifetime.

5 Conclusion

Lifetime assessment of plasma facing components for fusion reactor is of major interest. Such components are constituted of tungsten as material facing the plasma. Due to the thermal heat loading, tungsten microstructure changes. Once recrystallized, plasma facing material has weaker mechanical properties. The aim of this paper is to propose a numerical model implemented in ANSYS able to take into account the progressive change of the tungsten mechanical properties under thermal heat loading and to estimate the induced accumulated equivalent plastic strain increment for the life time assessment. This tool is named RXMAT. It takes into account the recrystallization kinetics and elastic-viscoplastic mechanical behaviour of tungsten and recrystallized tungsten. To model the recrystallized fraction within the plasma facing material, the anisothermal Johnson-Mehl-Avrami-Kolmogorov model formulation is used. The link between accumulated equivalent plastic strain increment and number of cycles to failure is estimated with common Manson Coffin laws. To propose probably more accurate life time assessment, fatigue data obtained for the temperature range relevant for the plasma facing material operation and for the relevant tungsten grades could be implemented in RXMAT. RXMAT is a parallel elastic-viscoplastic model which considers that the total strain is equal in the two model branches (for the as-received and the recrystallized material). One of the RXMAT specificity resides in the fact that the accumulated equivalent plastic strain increment is estimated from a mixture law. For the first time, it is possible to link numerically the evolution of the tungsten recrystallized fraction to a field of stresses and strains at each time step. First RXMAT applications highlight that the equivalent accumulated plastic strain increment depends on the recrystallized fraction, on the recrystallized fraction gradient and on elastic-viscoplastic parameters. The time required to recrystallize has consequently a direct impact on the component lifetime. These initial results suggest several applications. These would allow, for example, a better understanding of the geometry and recrystallization kinetics influence on the equivalent plastic strain accumulation within the component and especially within the tungsten block. RXMAT could also be used to study the component damage process exposed to complex thermal flux, representative of the fusion reactor environment. These perspectives let RXMAT to be a usable tool to help material and component design.

6 Acknowledgments

This work has received CEA funding from the "Programme Transverse de Compétence, Matériaux et Procédés (PTC-MP)". This work has been carried out within the framework of the EUROfusion Consortium and has received funding from the Euratom research and training program 2014-2018 under grant agreement No 633053. The views and opinions expressed herein do not necessarily reflect those of the European Commission.

A Appendix: Resolution method

Let's consider a time step$[t, t + \Delta t]$ and let's note with a subscript 0 the quantities and material constants at time t and without subscript, those at time $t + \Delta t$. At the beginning of the time step, all the quantities at time t are supposed to be known as well as the temperature, the thermal strain, the recrystallized fraction and the total strain tensor at time $t + \Delta t$. We also note with the symbol Δ, the increment of quantities during the time step. From equations 3 and 5, we first define σ^e, the stress tensor at time $t+\Delta t$ calculated supposing the behavior strictly elastic during the time step $[t, t + \Delta t]$:

$$\sigma^e = \lambda(tr(\varepsilon) - 3\varepsilon^{th})I - 2\mu(\varepsilon - \varepsilon_0^p) \tag{30}$$

The integration of equation 15 between t and $t+\Delta t$ combined with equation 12 gives:

$$\chi = \frac{X_0}{X}\frac{H}{H_0}\chi_0 + \frac{2}{3}H(\varepsilon^p - \varepsilon_0^p) \tag{31}$$

Let's now define from equation 31, χ^e, the kinematic variable at time $t+\Delta t$ if no plasticity occurs during the time step:

$$\chi^e = \frac{X_0}{X}\frac{H}{H_0}\chi_0 \tag{32}$$

If $J(\sigma^e - \chi^e) - \sigma^y \leq 0$, the behavior is actually elastic during the time step and we have $\sigma = \sigma^e$, $\varepsilon^p = \varepsilon_0^p$ and $\chi = \chi^e$.

If $J(\sigma^e - \chi^e) - \sigma^y > 0$, plasticity occurs during the time step.

From equations 9 and 30, the stress deviator S can be written:

$$S = S^e - 2\mu\Delta\varepsilon^p \tag{33}$$

where S^e is the deviator of σ^e.

From equation 6, it follows:

$$\Delta\varepsilon^p = \frac{3}{2}\Delta p\frac{(S - \chi)}{J(S - \chi)} \tag{34}$$

And from equation 31 and 32:

$$\chi = \chi^e + \frac{2}{3} H \Delta\varepsilon^p \tag{35}$$

Combining equations 33, 34 and 35, we obtain:

$$S - \chi = S^e - \chi^e - (3\mu + H)\Delta p \frac{(S - \chi)}{J(S - \chi)} \tag{36}$$

and then:

$$(1 + (3\mu + H)\frac{\Delta p}{J(S - \chi)})(S - \chi) = S^e - \chi^e \tag{37}$$

which shows that $S - \chi$ and $S^e - \chi^e$ are co-linear. Taking the von Mises function of the two members of equation 37 this gives:

$$J(S - \chi) = J(S^e - \chi^e) - (3\mu + H)\Delta p \tag{38}$$

Equation 6, with 10 and 38, then defines Δp as the solution of the following equation:

$$F(\Delta p) = \Delta p - (\frac{(J(S^e - \chi^e) - (3\mu + H)\Delta p - \sigma^y)}{K}) = 0 \tag{39}$$

Equation 39 is solved using a Newton method. Once known Δp, equation 34 with 37 and 38 gives $\Delta\varepsilon^p$ and then $\varepsilon^p = \varepsilon_0^p + \Delta\varepsilon^p$, and 35 gives χ.

B Appendix: Mesh sensitivity analysis

The figure 14 highlights the evolution of p over the first two millimeters of the depth of the block after 5 thermal cycles at 20 MW / m^2 as a function of different meshes. This study is carried out by changing the number of elements in a volume of 2 * 2 * 2 mm^3 around the node considered in this study (node max figure 7) . The numerical results presented in section 4 are attributed to the mesh called ref (figure 14) composed of 2.5 elements between the surface of the block exposed to the flow and 2mm deep. There is a maximum difference in the order of 9% depending on the meshes used. This observation is also valid for X (figure 15). These results reveal that the numerical simulations carried out within the framework of this study are robust. The reference mesh (ref) can be considered in the numerical studies.

References

1. A. Grosman et al, The WEST programme: Minimizing technology and operational risks of a full actively cooled tungsten divertor on ITER, Fusion Engineering and Design 88 (2013) 497– 500
2. E. Visca et al, Manufacturing and testing of ITER-like divertor plasma facing mock-ups for DEMO, Fusion Engineering and Design 136 (2018) 1593-1596

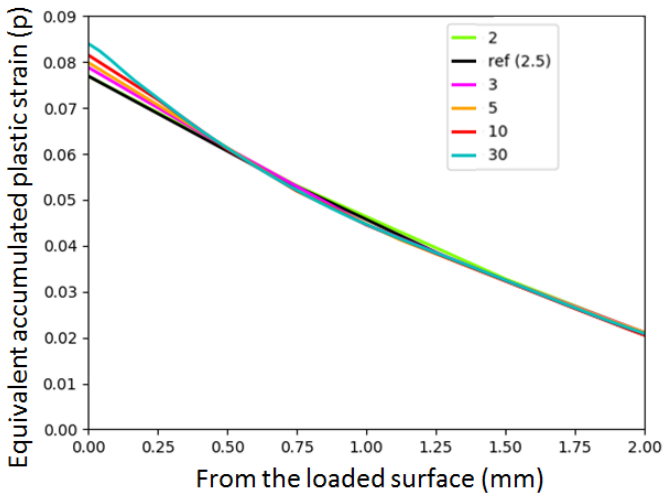

Fig. 14 Estimation of p between the loaded surface and 2mm depth after 5 thermal cycles at 20 MW/m^2

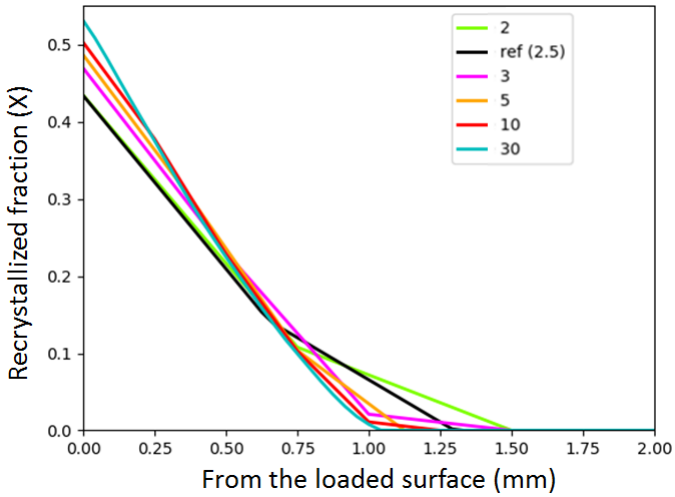

Fig. 15 Estimation of X between the loaded surface and 2mm depth after 5 thermal cycles at 20 MW/m^2

3. T. Hirai et al, "Status of technology RD for the ITER tungsten divertor monoblock" , Journal of Nuclear Materials 463 (2015), pp. 1248 - 1251. Plasma-Surface Interactions 21.
4. ITER, Heat and nuclear load specifications, d2luldhv 2.3 (16 Nov. 2009)
5. T. Hirai et al., "Use of tungsten material for the ITER divertor," Nucl. Mater. Energy.
6. S.Panayotis et al, Fracture modes of ITER tungsten divertor monoblock under stationary thermal loads, Fusion Engineering and Design 125 (2017) 256-262.
7. Nogami et al, Delegation of tungsten monoblock divertor under cyclic high heat flux loading. Fusion Engineering and Design (2017), 120 : 49-60.
8. G. Pintsuk et al., Characterization of ITER tungsten qualification mock-ups exposed to high cyclic thermal loads, Fusion Eng. Des., vol. 9899, pp. 13841388, Oct. 2015.

9. K. Ezato et al., “Progress of ITER full tungsten divertor technology qualification in Japan,” Fusion Eng. Des., vol. 98–99, pp. 1281–1284, Oct. 2015.
10. P. Gavila et al., “High heat flux testing of mock-ups for a full tungsten ITER divertor,” Fusion Eng. Des., vol. 86, no. 9–11, pp. 1652–1655, Oct. 2011.
11. B.Riccardi et al, “Preliminary results of the experimental study of PFCs exposure to ELMs-like transient loads followed by high heat flux thermal fatigue,” Fusion Eng. Des., vol. 86, no. 9–11, pp. 1665–1668, Oct. 2011.
12. G.Pintsuk et al, “Qualification and post-mortem chracterization of tungsten mock-ups exposed to cyclic high heat flux loading, Fusion Engineering and Design 88 (2013), 1858-1861
13. S.Panayotis et al, “Self-castellation of tungsten monoblock under high heat flux loading and impact of material properties, Nuclear Materials and Energy 12 (2017) 200-204
14. M. Li and J.-H. You, “Interpretation of the deep cracking phenomenon of tungsten monoblock targets observed in high-heat-flux fatigue tests at 20 MW/m^2,” Fusion Eng. Des., vol. 101, pp. 1–8, Dec. 2015.
15. A.Durif et al, “Impact of tungsten recrystallization on ITER-Like components for lifetime estimation”, Fusion Engineering and Design 138 (2019) 247-253.
16. J.Farre et al, Etude de la transition fragile-ductile du tungstène. J. Phys. IV France, 07: C3-879-C3-884.
17. J.Reiser et al, Tungsten foil laminate for structural divertor applications - tenseile tests properties of tungsten foil. Journal of Nuclear Materials, 434 (1) : 357-366. Special Section on Spent Nuclear Fuel.
18. A.Durif, “Modélisation de la durée de vie de composants face au plasma dans les réacteurs à fusion thermonucléaire”, Ph.D Thesis. Thèse de Doctorat Mécanique et Ingénierie (2019), ref: 2019LYSEE005, [on line 08/05/2020: http://www.theses.fr/2019LYSEE005/document]
19. ITER Structural design criteria for in-vessel components (SDC-IC) appendix A: Materials design limit data , g74ma, 8 01-05-28w0.2, 2013
20. J-M.Bergheau (2014),Thermomechanical Industrial Processes: Modeling and Numerical Simulation. ISTE. Wiley
21. ITER Material Properties Handbook, ITER document $N°S74MA2$
22. J.Lemaitre and J.Chaboche (2004). Mécanique des matrériaux solides. Sciences SUP. Science de l’ingénieur. Dunod.
23. J.-M Bergheau, G. Mottet, O. Débordes, ”Intégration numérique de lois de comportement élastoviscoplastique endommageable et applications”, Revue Européenne des Eléments Finis, Taylor & Francis, Vol.7, $n°6$, 1998, pp.681-708
24. J.-B. Leblond, Mathematical modelling of transformation plasticity in steels II: Coupling with strain hardening phenomena, Int. J. Plasticity, 5 (6), 1989, 573-591
25. W.Bahm (2005). Nuclear fusion programme annual report of the assiociation Forschungszentrum Karlsruhe / euratom, January 2004 - December 2004. Technical report. 31.00.00; LK 01; Wissenschaftliche Berichte, FZKA-7117 (May 2005) EUR-21526-EN
26. F.J. Humphreys and M.Hatherly (2004). Recrystallization and related annealing phenomena (second edition).
27. W.A. JOHNSON and R.F. MEHL, ”Reaction kinetics in process of nucleation and growth”. Trans. AIME, 135, p. 416-458 (1939).
28. M.Avrami, -Kinetics of phase change. I: General theory. II: Transformation-time relations for random distribution of nuclei. III: Granulation, phase change and microstructure. J. Chem. Phys., 7, p. 1103-1112 (1939) ; 8, p. 212-224 (1940) ; 9, p. 177-184 (1941).
29. Poster presentation at the 13th International Workshop on Plasma-Facing Materials and Components for Fusion Applications, Rosenheim, 09-13 May 2011, Germany
30. Alfonso Lopez, A., Pantleon, W., Juul Jensen, D., & Luo, G. (2015). Thermal stability of warm-rolled tungsten. DTU Mechanical Engineering.
31. F.M.Fernandes and S.Denis and A.Simon, “Mathematical model coupling phase transformation and temperature evolution during quench of steels. Mat. Sci. Technol., Vol 10, p.838-844, 1985
32. W.I. Pumphey et al, ”Inter-relation of hardenability and isothermal transformation data”, JISI, vol.159, p.137-144, 1948

33. J-B. Leblond and Devaux, "A new kinetic model for anisothermal metallurgical transformations in steel including effect of austenite grain size". Acta Metallurgica, 32, 1 p. 137-146 (1984)
34. M.Richou et al, "Recrystallization at high temperature of two tungsten materials complying with the ITER specifications", Journal of Nuclear Materials [under publication]
35. F. Saint-Anthonin (1997). Essais de relaxation isotherme. Techniques de l'ingénieur Essais mécaniques sur les métaux et alliages, base documentaire: TIB387DUO
36. G.Kermouche. "Contribution à la modélisation théorique et numérique des essais d'indentation et de rayure". Ph.D Thesis. Thèse de Doctorat Mécanique Lyon (2005)
37. T.Oda, "Thermodynamic model for grain boundary effects on hydrogen solubility, diffusivity and permeability in poly-crystalline tungsten", Fusion Engineering and Design 112 (2016) 102-116.
38. Y.Charles et al, "Adaptation of hyfrogen transport models at ht polycrystal scale and application to the U-bend test", Procedia Structural Integrity 13 (2018) 896-901